Mon. Not. R. Astron. Soc. **272**, 665–677 (1995)

A *ROSAT* PSPC investigation of NGC 1399: cold gas and cooling flows in elliptical galaxies

F. V. N. Rangarajan,[1] A. C. Fabian,[1] W. R. Forman[2] and C. Jones[2]

[1] *Institute of Astronomy, Madingley Road, Cambridge CB3 0HA*

[2] *Smithsonian Astrophysical Observatory and Harvard–Smithsonian Centre for Astrophysics, 60 Garden Street, Cambridge, MA 02138, USA*

Accepted 1994 September 20. Received 1993 December 9; in original form 1994 May 19

ABSTRACT

ROSAT PSPC observations of the Fornax cluster reveal an isothermal gaseous medium at radii from 10 to 330 kpc, with a temperature of 1.1 ± 0.1 keV using Raymond–Smith (RS) models and 0.9 ± 0.1 keV using Mewe–Kaastra (MEKA) models. Within 10 kpc the temperature falls to 0.85 keV (RS) or 0.6 keV (MEKA). The surface brightness is well fitted by a cooling flow model with a mass deposition rate of at least $2\,M_\odot\,yr^{-1}$, mostly within the galaxy itself. The abundance is consistent with solar, and the mass of hot X-ray-emitting gas out to 46 kpc is over $10^{10}\,M_\odot$. The MEKA models show clear evidence of an absorbing column density greater than 10^{21} cm^{-2} in the centre of NGC 1399, and the variation of column density with radius implies a mass of cold gas in the galaxy of $1.6 \times 10^{10}\,M_\odot$ within 40 kpc, and a mass deposition profile $\dot{M} \propto r$. Within 10 kpc of the centre of NGC 1399, the mean density of cold absorbing gas is similar to that of the hot gas. Using a deprojection method, the density and pressure in the gas are calculated, and other physical parameters of the gas derived. This combination of analyses is used to constrain the gaseous history of NGC 1399. We set a limit on the X-ray flux of the radio source.

Key words: ISM: general – cooling flows – galaxies: elliptical and lenticular, cD – galaxies: individual: NGC 1399 – galaxies: ISM – X-rays: ISM.

1 INTRODUCTION

NGC 1399 is the central galaxy in the Fornax cluster of galaxies, a poor cluster about 27 Mpc away ($H_0 = 50$ km s^{-1} Mpc^{-1}). It has a close, non-interacting companion 10.2 arcmin to the south-east, NGC 1404. Observations show many globular clusters (Bridges, Hanes & Harris 1991), in a faint extended corona, and a two-lobed radio source (Sadler, Jenkins & Kotanyi 1989), with the lobes contained within the galaxy and probably pressure-confined by the interstellar medium (ISM) (Killeen & Bicknell 1988b). The Galactic H I column density to NGC 1399 $\sim 1.3 \times 10^{20}$ cm^{-2} (Stark et al. 1992), and the redshift of the galaxy is 0.004 17, corresponding to a velocity of 1422 km s^{-1} (Roberts et al. 1991), and a scale of 1 arcmin ~ 7.7 kpc.

This paper describes the spectral analysis and deprojection of a *ROSAT* Position Sensitive Proportional Counter (PSPC) observation of NGC 1399 and the surrounding intracluster medium. In Section 2, we present the spectrally derived temperature and absorption results and, in Section 3, the physical parameters of the gas in the galaxy, derived by deprojection. In Section 4, we show what the expected amount of absorption would be, given the expected rate of stellar mass loss and the mass deposition rate of the cooling flow, and relate that to the amount detected.

1.1 Previous observations

Killeen & Bicknell (1988a) used blue and red photographic plates and the *Einstein* Imaging Proportional Counter (IPC) 0.5–4.5 keV X-ray spectral images of the cluster to model the X-ray-emitting gas using different gravitational potentials. Because of the effective area and sensitivity of the IPC, they did not have a well-constrained temperature profile; thus they find that both isothermal models (with $T \sim 10^7$ K and no dark matter, or a higher temperature and dark matter) and polytropic models (with a higher temperature and dark matter) fit well. At large radii (> 26 kpc) they had only a lower limit to the temperature ($T > 3 \times 10^6$ K), and the temperature at this radius has to be the minimum allowed for a fit with no dark matter. They also find that the radio source in the centre is likely to be confined by the thermal pressure of the ISM. Their constraint is $kT \sim 1.5$–5.6 keV in the central 26 kpc.

Kim, Fabbiano & Trinchieri (1992) also analysed the *Einstein* IPC data, finding $kT > 1.1$ keV, with little constraint on how high it can be, and $10^{20} < N_H < 10^{21}$ cm^{-2}.

White (1992) deprojected the *Einstein* High Resolution Imager (HRI) data, and found a cooling flow of 0.8 ± 0.6 $M_\odot$ yr^{-1}, assuming a temperature of the order of 10^7 K. The data were also deprojected, with assumptions about the supernova energy input and stellar mass injection (Thomas et al. 1986).

Ikebe et al. (1992) have used the *Ginga* satellite to observe NGC 1399 and the region around it, finding $kT \sim 1.25$–1.51 keV and a solar abundance, but it seems likely that the single temperature measured is primarily from the cluster, because of the large field of view of the telescope.

The Broad Band X-ray Telescope (BBXRT) observed Fornax from the Shuttle (Serlemitsos et al. 1991, 1993), and detected a temperature drop in the inner 14 kpc, finding $kT \sim 1.0$–1.1 keV in the central pixel and $kT \sim 1.1$–1.2 keV in the outer pixels, at about 50 kpc off-axis. Their data require N_H to be 10^{20}–10^{21} cm^{-2} above the Galactic value in all pixels. A harder component, modelled with a 6-keV bremsstrahlung component, improved their fits. This could be due to X-ray binaries, and partly due to supernova remnants. They find that the abundance is highly model-dependent, $\sim 0.5 \pm 0.3$ solar, but it is always less than solar.

Jenkins (1983) observed Fornax, using the Parkes 64-m telescope, and found the H I mass to be $M(\mathrm{H\,I}) < 10^8$ $M_\odot$.

Observations by the *IRAS* satellite (Jura 1986) showed a mass of cold gas $\sim 0.91 \times 10^8$ $M_\odot$, assuming a Galactic dust-to-gas ratio.

Hopkins Ultraviolet Telescope (*HUT*) observations (Ferguson et al. 1991) examined the UV upturn in NGC 1399. Most of the flux in the *HUT* bandpass comes from stars with main-sequence lifetimes that are less than a few times 10^7 yr. The authors argue that the observed lack of C IV absorption is only explicable if B0 stars define the current main-sequence turnoff. Their comparison of the spectra around C IV to model spectra of star formation over the last 10^8 yr shows that either star formation ended $\sim 2 \times 10^7$ yr ago, or is currently happening with a truncated IMF.

Using blue Schmidt plates from the ESO/SRC survey, no morphological evidence for dust has been found in NGC 1399 (Sadler & Gerhard 1985). The galaxy is highly spherical [$\log(a/b) = 0.000$], and has one of the largest angular effective radii of their sample, increasing the chances of detecting a dust lane if one exists.

1.2 *ROSAT* PSPC observations

The PSPC observation of the Fornax cluster was made on 1991 August 14, with a total on-source exposure of 15 292 s. The pointing of the observation, at RA 54°.62 and Dec. −35°.45 (J2000.0), and a field of view of 1°.6, was well centred on NGC 1399, as shown in Fig. 1.

2 SPECTRAL ANALYSIS AND RESULTS

2.1 Spectral model and background subtraction

The data were vignetting-corrected and rebinned, but not background-subtracted because of the presence of the cluster emission over the whole field of view. All other sources detectable in the image were masked out, including NGC 1404. An annulus centred on the peak of emission of NGC 1399, inner radius 0°.6, outer radius 0°.7, was chosen to act as a background region. This annulus is well away from the galaxies, largely free of point sources, and at the largest radius where the energy-dependent vignetting correction is understood. Use of a smaller annulus would increase the signal-to-noise ratio of the source component, decreasing the sensitivity of the background component fits, and might increase the complexity of the model spectrum needed. The spectrum from this area had 1 per cent systematic errors added in quadrature, and was fitted with the background model and a single-temperature, optically thin source plasma (Raymond & Smith 1977, hereafter RS), with absorption held to the Galactic value. When the spectrum was fitted with a model with the column density and all background parameters variable, the column density was consistent with the Galactic value, but, because of the low signal-to-noise ratio at these large radii, the constraint on the column is only order-of-magnitude. The background model follows Hasinger (1992) and Allen & Fabian (1994) with three components: (i) a 10^6 K (80.8 eV) RS thermal plasma with no absorption; (ii) a 2.5×10^6 K (0.2 keV) RS thermal plasma with known flux, temperature and absorption of 5×19^{19} cm^{-2}; and (iii) a power law with known photon index and flux $F = a\nu^{-1.12}$, where ν is frequency, and a is normalized such that the unabsorbed flux at 1 keV is 13.4 keV cm^{-2} s^{-1} sr^{-1} keV^{-1}, with a column density the sum of Galactic and source absorption. The known fluxes were scaled from the average values obtained from deep pointings by Hasinger.

The 10^6 K flux varies strongly over the sky, but a comparison of opposite quadrants of the background annulus indicates that the variation in this observation is less than 20 per cent across degree scales.

The background components of the model for the 0°.6–0°.7 annulus were fixed, and thereafter were always scaled together. Spectra were generated from the other source-subtracted annuli, and had 1 per cent systematic errors added in quadrature. These were then fitted with the background model, with fluxes scaled for the differing areas, and a source model. The same background model was used for all tests.

2.2 MEKA spectral models

The data were also fitted with spectra derived from the plasma models of Mewe, Gronenschild & van den Oord (1985) and Kaastra, hereafter MEKA models (Kaastra & Mewe 1993a,b). These differ from the RS models in their treatment of several line energies and equivalent widths, and in the use of different ionization and electron cascade parameters, and a different set of cosmic abundances (Anders & Grevesse 1989). The major abundance changes are given in Table 1, the most important of which is that the iron abundance in the MEKA models is 1.48 times the value in the solar-abundance RS models, relative to hydrogen.

The fits were done for an abundance of 1 (where the iron is 1.5 times the RS value), an abundance of 0.66 (iron as in RS at solar abundance, other elements less), and variable abundance. In general, the abundances fit to within about 0.8 of the MEKA solar values, but they are only constrained to about ± 0.3.

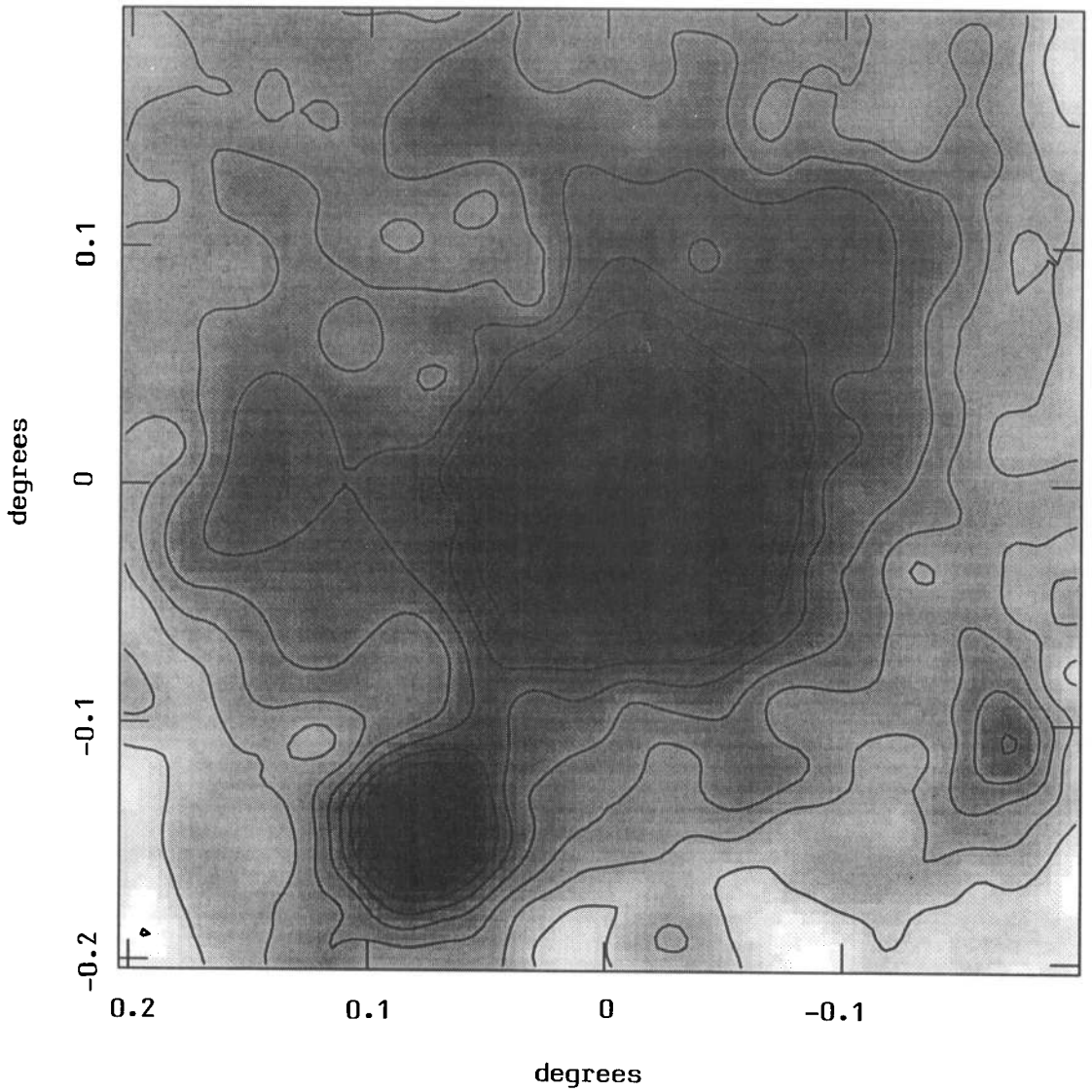

Figure 1. Flux contours of the *ROSAT* PSPC image of NGC 1399, overlaid on a grey-scale representation. The total exposure is 15 292 s, and the image has been smoothed but not corrected for vignetting. NGC 1399 is well centred in the exposure, with NGC 1404 lying 10 arcmin to the south-east.

2.3 RS spectral results

This investigation was primarily to explore the conditions of the gas in the inner 46 kpc of the cluster, where it is essentially inside the galaxy. First, a simple, one-temperature RS source plasma with Galactic absorption was fitted to the spectrum from the inner 46 kpc from 0.2 to 2 keV. This gives a reduced chi-squared statistic $\chi^2/\nu \sim 2$ with a soft excess, in observed flux over the model, of about 16 per cent in the range 0.2–0.3 keV. Rejecting this model because of its poor fit to the soft flux, we then allow the column density to vary, but this gives $9.9\times10^{19} < N_{\rm H} < 1.4\times10^{20}$ cm^{-2} at 90 per cent significance, inconsistent with a Galactic column of 1.3×10^{20} cm^{-2} (Stark et al. 1992), as shown in Fig. 2.

There are known problems with the normalization of the *ROSAT* PSPC response matrix in the 0.2–0.4 keV PHA channels, at the 2–3 per cent level, which could be the cause of this soft excess. To test whether this could explain the soft excess, spectra were generated with 4 per cent systematic errors added in quadrature (representative of the maximum likely error), and these were fitted with the same models as above. The excess still appears, and it is still statistically significant to add an extra parameter to fit it better.

To fit the soft excess we need to introduce an extra soft-emission component, which we model using a 80.8-eV RS thermal component, with solar abundance. The introduction of the soft component does not affect the temperature determination for the main thermal component (~ 1 keV), but it does affect the column density allowed. Fig. 2 shows the confidence contours for the two parameters involved, the flux of the soft component and the absorption on the whole two-temperature source model. This shows that the column density is inconsistent with Galactic column without the extra soft flux. With the soft flux allowed to vary in the fit, the absorbing column can be up to 1.4×10^{20} cm^{-2} above Galactic absorption at 1.3×10^{20} cm^{-2}. In the central 10 kpc

Table 1. Comparison of RS and MEKA model abundances.

Element	RS abundance	MEKA abundance
H	1.0000	1.0000
He	0.0977	0.0977
C	3.31e-4	3.63e-5
N	9.12e-5	1.12e-4
O	6.61e-4	8.51e-4
Ne	8.32e-5	1.23e-4
Na	-	2.14e-6
Mg	2.63e-5	3.80e-5
Al	-	2.95e-6
Si	3.31e-5	3.55e-5
S	1.58e-5	1.62e-5
Ar	7.94e-6	3.63e-6
Ca	2.00e-6	2.29e-6
Fe	3.16e-5	4.68e-5
Ni	2.00e-6	1.78e-6

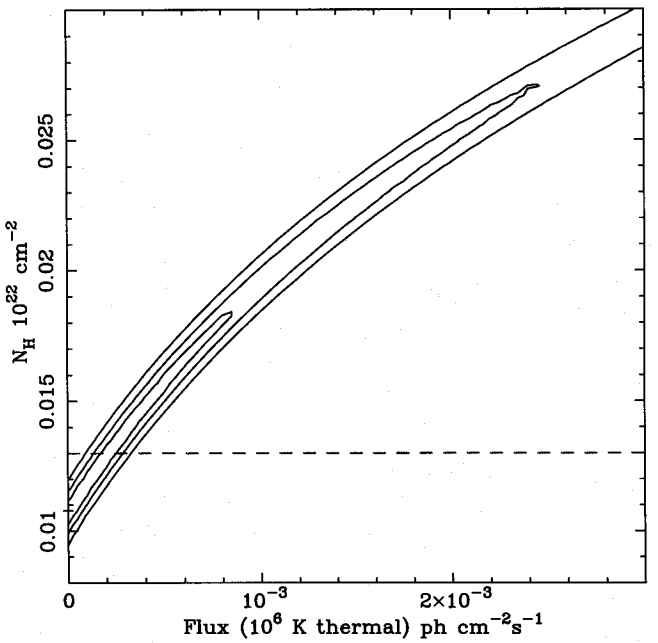

Figure 2. Contours of $\Delta\chi^2$ for the total absorbing column in the RS spectral model for NGC 1399 versus the soft (10^6K) component normalization. Contours are at $\Delta\chi^2 \sim 2.3$, 4.61 and 9.21. Note that without any soft flux the absorption is inconsistent with a Galactic column density of 1.3×10^{20} cm^{-2}.

a similar treatment allows up to 3.2×10^{20} cm^{-2} above Galactic. The point spread function of the PSPC at 80 eV is below 1 arcmin (Turner & George 1992), but the soft component is needed over the whole central 40 kpc (6 arcmin), and so it cannot be produced by a single point source.

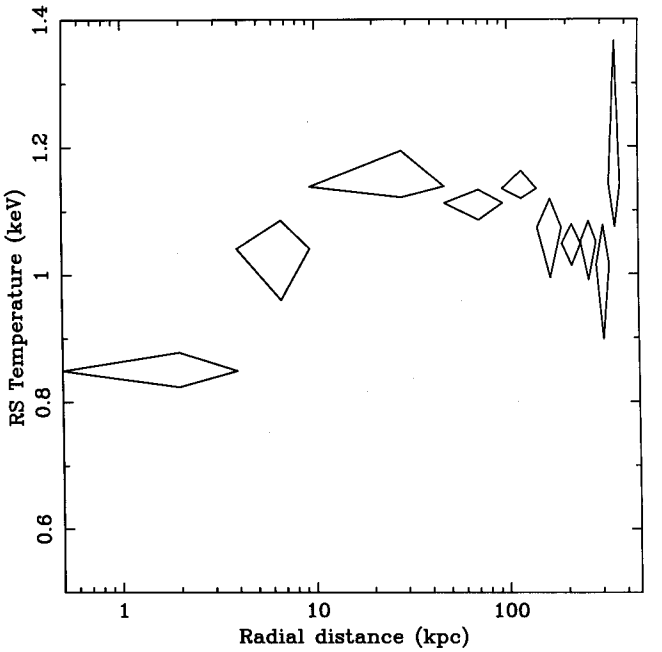

Figure 3. Temperature profile derived by spectral analysis from the *ROSAT* PSPC observation of NGC 1399, when fitting a two-temperature RS model with variable absorption and a 6-keV bremsstrahlung component. Errors bars are at 90 per cent significance.

The 6-keV bremsstrahlung emission seen by BBXRT is not needed statistically in any annulus, but helps the fit (*F*-test parameter ~ 1.9 in the inner 9 kpc), and can be attributed to the combined emission of X-ray binaries, and possibly supernova remnants. It reduces χ^2 slightly in the inner 6 arcmin (46 kpc), and is definitely not required in any other annulus, arguing that it has a physical origin, and is not a background-fitting error. The flux is consistent with that found by BBXRT, providing ~ 8 per cent of the luminosity in the 0.2–2.0 keV band. The inclusion of the bremsstrahlung component does not affect the temperature profile derived (Fig. 3). Thus we include it in our most likely model.

We find no significant abundance gradient in the spectra, from 300 kpc into the centre. The abundance is typically constrained to better than 20 per cent at 90 per cent confidence, and is always consistent with being solar. This agrees with the *Ginga* results, and is just consistent with the BBXRT abundance (at 90 per cent) if a two-temperature fit is used for the BBXRT data, but is inconsistent with the abundance derived by a BBXRT single-temperature fit.

Several other models were tried. (i) Partial covering by absorbing material (in addition to Galactic) on the soft RS thermal plasma. This is statistically not required – in general, the model spectra need more unabsorbed very soft emission, not more absorbed harder emission. (ii) A soft thermal plasma with extra fully covering absorption – the spectral resolution of the *ROSAT* PSPC is not sufficient to distinguish the characteristics of this using the five effective spectral channels available, and the fits are unstable, with unconstrained error bars.

The limits on partial covering were tested by generating model spectra resembling the inner 46 kpc, using a two-temperature RS plasma and various forms of absorption.

These show that the spectral response of the detector is not fine enough to distinguish between full and partial covering by absorbing material. Spectra generated with full covering can be fitted equally by partial covering models, but the change in goodness of fit is insignificant, and the error bars are large. Spectra generated with partial covering can be fitted with full covering, and this produces an underestimate of the column density by about an order of magnitude. The fits to simulated partial covering spectra are not significantly improved by using a partial covering model. This difficulty in fitting partial covering models is due to the low temperature of the plasma observed, which places the energies where absorption is most easily detectable in the 0.4–0.7 keV band of the instrument, where the sensitivity is less due to the carbon edge. Thus more absorbing gas than these limits suggest could be in the galaxy, if it forms a screen of partially covering, high-optical-depth, clumpy absorption.

The centre of NGC 1399 houses a weak radio source, but this is not detectable in the X-ray spectra extracted from any of the central 6, 1.2 or 0.5 arcmin of the galaxy. A power-law component was added to the model spectra, but the flux is always consistent with zero. Using the spectrum from the innermost 4 kpc, the X-ray flux (0.2–2 keV) of the active nucleus is less than 2.4×10^{-13} erg cm^{-2} s^{-1} at 90 per cent confidence, corresponding to a limit on the de-absorbed band luminosity of 2×10^{40} erg s^{-1} at source.

In conclusion, no extra X-ray-absorbing column density is detected in the outer regions of this cluster, outside the central galaxy. The spectrum from the central 46 kpc demands extra soft emission in order to be consistent with the Galactic column density. If this soft flux is modelled by a 10^6-K RS plasma, then the column can be up to 1.3×10^{20} cm^{-2} above Galactic. In the central 10 kpc a similar treatment allows up to 3.2×10^{20} cm^{-2} above Galactic. A higher column density (over 10^{21} cm^{-2}) is possible if the absorbing gas only covers the source plasma partially. The abundances measured out to 350 kpc are consistent with no abundance gradient. We do not detect X-ray emission from the radio nucleus.

2.4 MEKA model spectral results

The physical parameters generated by fitting MEKA plasma spectral models are different from those obtained using RS models, due to the different recombination rates, electron cascade rates and number of emission lines used (Arnaud & Raymond 1992). The MEKA models often give significantly better fits than the RS models, with χ^2 much lower. Both the temperature of the hot component (see Fig. 4) and the abundances are lower. In a similar way to the RS fits, the model of the inner 40 kpc still produces too little soft emission, thus forcing the fitted absorption to be too low, and we need a very soft (~ 0.1 keV) component to fit acceptable absorptions. The lack of soft emission in the model is not corrected by varying the abundance (this increases the iron L lines at ~ 1 keV as well as at 0.1 keV and disturbs the goodness of fit around 1 keV), nor by varying the absorption, as this makes it incompatible with Galactic $N_{\rm H}$ (the fitted models prefer less absorption, to boost the soft flux in the model, and the 90th percentile upper limit on the column density falls to 1.0×10^{20} cm^{-2} – well below Galactic).

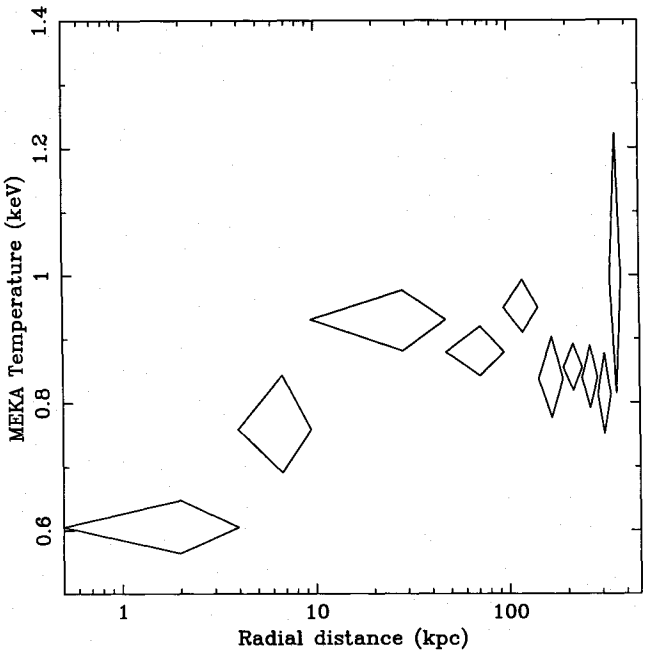

Figure 4. Temperature profile derived by spectral analysis from the *ROSAT* PSPC observation of NGC 1399, when fitting a two-temperature MEKA model with variable absorption and a 6-keV bremsstrahlung component. Errors bars are at 90 per cent significance.

Another possibility is the existence of a cooling flow in the centre of the galaxy, which contains gas at a wide spectrum of temperatures. This was modelled using an integration of MEKA spectra over a temperature interval, weighted by emission measure. The highest temperature is that of the hot component, and the lowest temperature is set below detectable thresholds. This model is not required by the χ^2 fits unless extra absorption is added on to the cooling flow component alone, but if all parameters are free this produces so little soft emission that the absorption on all components falls and is inconsistent with the Galactic value. However, it is possible to fit spectra from the inner 40 and 10 kpc with simple cooling flow spectra including extra absorption, an absorption on other components consistent with Galactic, and a similar soft emission component to the simple MEKA models above. The reduced chi-squared is acceptable ($\chi^2/\nu = 1.1$). The mass deposition rate in the inner 40 kpc is $\dot{M} \sim 1.6$ M$_\odot$ yr^{-1}, and up to 1 M$_\odot$ yr^{-1} in the inner 10 kpc, and the absorbing column is very similar to that found using the two-temperature models. However, because of the lack of spectral resolution, the solutions are degenerate, so while both cooling flow models (with extra soft emission) and simple two-component models fit acceptably, the errors on the model normalizations and the errors on the extra absorption are both indeterminate, and model fits unstable.

Models with high abundances (from 1 up to ~ 5) were also tried, to detect if the soft deficit in the model is due to a lack of the iron lines around 0.1 keV. These models are not statistically needed and if the abundance is allowed to vary then χ^2 is lower when it is subsolar (roughly equivalent to solar abundance in the RS models in iron), except for the

spectra from the innermost 10 kpc, where the abundance is indeterminable.

In the central 6 arcmin the flux from the bremsstrahlung component is 1.5×10^{-12} erg cm^{-2} s^{-1}, which contributes about 13 per cent of the total flux and between 6 and 20 per cent at 90 per cent confidence, again consistent with the BBXRT values.

A spectral ratio plot comparing spectra from different annuli (see Fig. 5) shows the clear effect of extra absorption in the centre of the galaxy. The spectra from 12 to 18 arcmin [94 to 140 kpc, panel (b)], the actual data, are compared with a simple unabsorbed MEKA model. The lower line is the spectrum from that annulus, with the background components subtracted, and shows single-temperature cluster emission with no extra column density – the flux below 0.4 keV is consistent with that emission and Galactic absorption, and the comparison MEKA spectrum [panel (b), upper line] is in almost perfect agreement down to 0.5 keV. The comparison spectrum is a MEKA model at the same temperature as the best-fitting main hot component fitted to the source spectrum, normalized to give the same flux as the source spectrum at the hardest energies, and with no absorption. The source spectrum from the inner 1.2 arcmin [10 kpc; panel (a), lower line], when compared with a similarly derived reference MEKA spectrum at the best-fitting temperature for that annulus [panel (a), upper line], shows the effect of absorption as high as 1.5 keV, which must be by a column density much higher than that on the 12–18 arcmin bin, of order 10^{21} cm^{-2}. A reduction of the temperature of the reference spectrum, to try to fit the source spectrum with a lower column density, does not give a statistically acceptable fit at any column density or abundance. To check that this extra absorption is not a model-dependent result, the spectrum from the inner 1.2 arcmin was fitted with a single-temperature model and variable absorption, using photons solely above 0.6 keV (so avoiding the soft model uncertainties below that). This fit needs a similar extra absorption to that of the whole spectrum, giving a column density of $2.6^{+0.41}_{-0.16} \times 10^{21}$ cm^{-2} (90 per cent errors) and a high (>99 per cent) significance that the column is greater than Galactic. Variation of the abundance does not improve the fit, and is statistically insignificant. *This demonstrates that the high* N_H *found to be necessary for the model of this spectrum is not an artefact of the background subtraction, nor of soft emission model inadequacies or PSPC soft calibration errors, but is needed to explain the shape of the flux at around 1 keV, where the errors are smallest.*

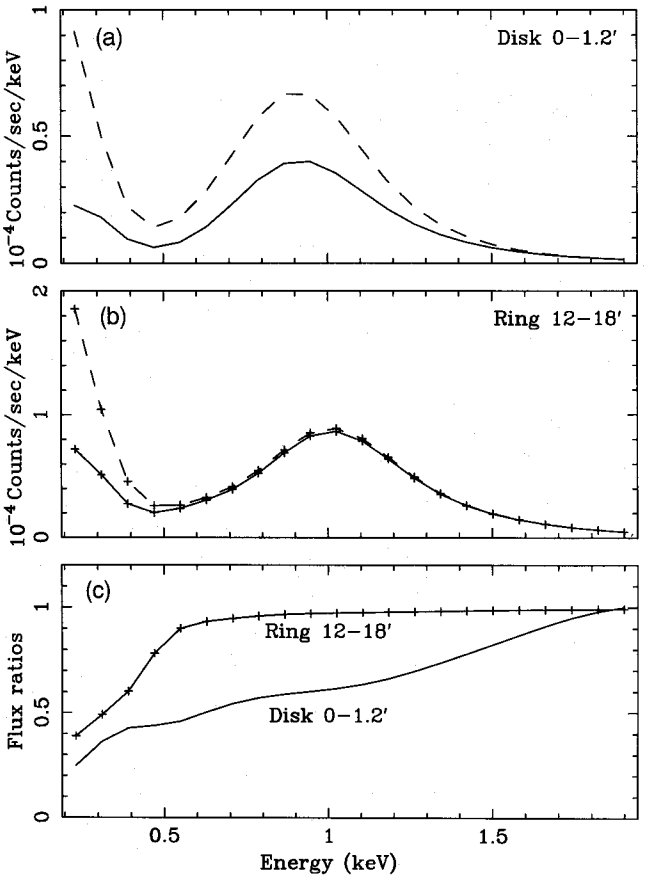

Figure 5. Spectral ratios derived by spectral analysis from the *ROSAT* PSPC observation of NGC 1399, when fitting a two-temperature MEKA model with variable absorption and a 6-keV bremsstrahlung component. (a) Background-subtracted spectrum from a circle radius 1.2 arcmin (~10 kpc) centred on the emission peak, and a comparison unabsorbed MEKA model spectrum (dashed line) of the same temperature as the hot thermal component, normalized at the highest energies. (b) Background-subtracted spectrum from the annulus between 12 and 18 arcmin (~100–150 kpc) from the centre of NGC 1399, and a comparison unabsorbed MEKA model spectrum (dashed line) of the same temperature as the hot thermal component, normalized at the highest energies. Units are 10^{-4} count cm^{-2} s^{-1} keV^{-1}. (c) Source spectrum divided by comparison MEKA spectrum for the two areas. The marked line is from 12 to 18 arcmin, the smooth line from the inner 1.2-arcmin disc. This clearly shows the effect of much higher absorption on the inner spectrum, removing more, and higher energy, photons.

An absorption profile for NGC 1399, derived using MEKA fits to the data (Fig. 6), shows the amount of extra absorption clearly and consistently. The spectrum emerging from the innermost 4 kpc requires an extra column density of $N_{\rm H} \sim 1.9^{+0.6}_{-1.0} \times 10^{21}$ cm^{-2} above Galactic; an extra $(7.5 \pm 6) \times 10^{20}$ cm^{-2} is needed on the emission from around 7 kpc, and an extra $1.4^{+1.8}_{-1.1} \times 10^{19}$ cm^{-2} on the emission from 30 kpc. The amount of absorption allowed on the spectrum from the whole inner 40 kpc fits to $3.5^{+1.9}_{-0.2} \times 10^{20}$ cm^{-2}, and within the whole inner 10 kpc $N_{\rm H} \sim (1.4 \pm 0.6) \times 10^{21}$ cm^{-2}, all at 90 per cent confidence. The absorption needed for models fitted to all data within 10 kpc (i.e., the two innermost spectra combined) is included in the plot to show that the high absorption derived in the very innermost bin is not an effect of the energy dependence of the instrument [soft photons are scattered more than hard ones over scales of about 1 arcmin because of the energy dependence of the point spread function (PSF)]. 10 kpc corresponds to 1.2 arcmin, so the 0–10 kpc bin is independent of this effect. It appears that the innermost bin is not greatly affected by the energy dependence of the PSF, and is a valid spectrum to use for analysing the absorption present. In this bin, the limit on a power-law X-ray flux with spectral index $\nu = 2.12$ from a central point is $\sim 1.8 \times 10^{-13}$ erg cm^{-2} s^{-1} (0.2–2 keV) at 90 per cent confidence, corresponding to a limit on the de-absorbed band luminosity of 1.5×10^{40} erg s^{-1} at source.

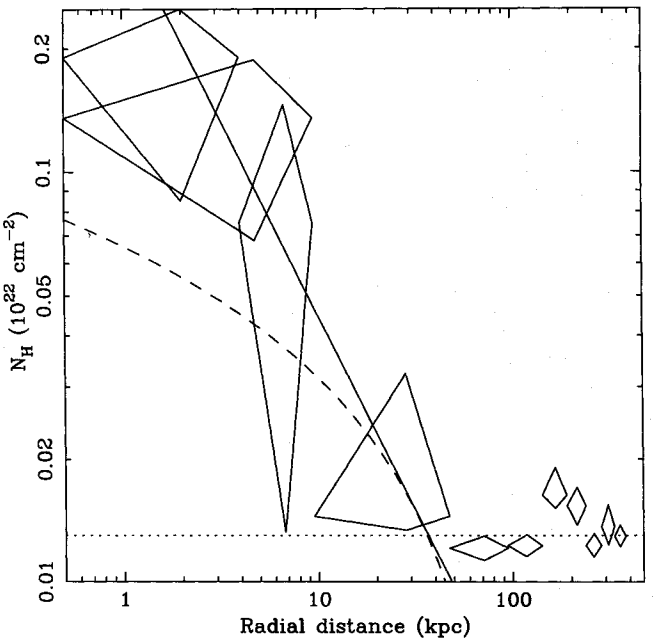

Figure 6. Absorption profile derived by spectral analysis from the *ROSAT* PSPC observation of NGC 1399, when fitting a two-temperature MEKA model with variable absorption and a 6-keV bremsstrahlung component. Errors bars are at 90 per cent significance. The solid line is a power-law fit to the absorption within 40 kpc. Galactic column density is 1.3×10^{20} cm^{-2}, marked on as a dotted line. The dashed line is the hot gas column density derived from deprojection analysis, and is normalized such that at 35 kpc, where the cold gas *excess* column is zero, the hot gas column is equal to the cold gas total column, to allow easy comparison between the column densities, looking in from 35 kpc.

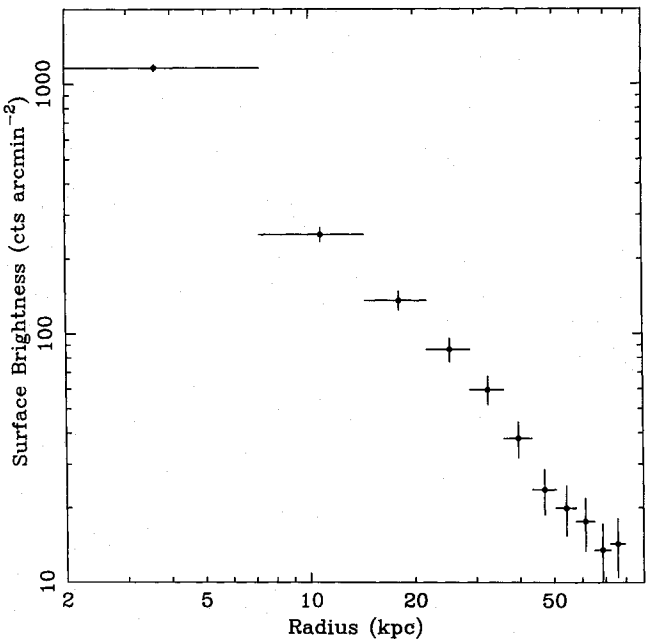

Figure 7. The X-ray surface brightness profile of NGC 1399, source-subtracted, vignetting-corrected, and binned into 2-arcmin bins. Errors bars are Poissonian.

3 DEPROJECTION ANALYSIS AND RESULTS

3.1 The deprojection method

Surface brightness profiles of the core of the cluster, azimuthally summed about the centroid of the galactic emission, were then deprojected following the method of Fabian et al. (1981) and White et al. (1994). This assumes that the X-ray image is formed by the projected emission of concentric spherical shells of X-ray-emitting gas. The assumption of spherical symmetry is valid here for the galaxy, as we measure the X-ray contours of NGC 1399 to have an ellipticity of less than 0.08 within 46 kpc. The counts from the outermost ring are assumed to come solely from the outermost shell, and thus the counts from the next interior ring can be calculated. This cumulative subtraction of outer emission produces the count-emissivity per unit volume of each radial shell.

The calculated count-emissivity is compared with the count rate from a model consisting of a thermal RS plasma absorbed by galactic material (with the cross-sections calculated by Morrison & McCammon 1983) and convolved with the detector response. The model counts are a function of plasma temperature, T, and electron density, n_e ($F\propto n_e^2 T^{1/2}/4\pi d^2$) for bremsstrahlung emission, where F is the flux observed, and d is the luminosity distance. The gas pressure is $P\propto n_e T$. Given a gas pressure and count-emissivity, T and n_e can thus be calculated. The gas pressure is specified in the outermost bin, and the pressure in inner bins can be determined using the given gravitational potential and the temperature and density of the gas in outer bins, assuming hydrostatic equilibrium in the gas ($\mathrm{d}P/\mathrm{d}r\propto -n_e\mathrm{d}\phi/\mathrm{d}r$, where ϕ is the gravitational potential). The pressure in the outermost bin is selected by comparing the resulting outer temperature with a spectrally determined temperature at the same radius. Note that, since the deprojection uses the RS code to determine the emissivity at each radius, we use the temperatures derived from the RS model fit to the spectra (Fig. 3) to normalize the deprojection temperature profile. The shape and depth of the gravitational potential determine the subsequent inner deprojection temperature profile, and we show that this can tightly constrain the gravitating mass distribution.

The uncertainties on the deprojection parameters are estimated using Monte Carlo perturbations of the surface brightness profile. The results are displayed as mean values and standard deviations, except for the temperature, cooling time and mass deposition rate. These parameters do not necessarily follow a symmetric distribution, so results are given as median values with 10th and 90th percentile limits.

3.2 Deprojection inputs and model

The deprojection uses an azimuthally averaged surface brightness profile of the galaxy, which is smooth and highly peaked in the centre (see Fig. 7). All point-like sources and NGC 1404 were masked from the image, which was binned into 1-arcmin wide annular bins about the centroid of the emission within a 20-kpc radius. The profile was then corrected for vignetting. The background subtraction is handled in the software, by subtracting the counts of the outermost bin at 130 kpc from all bins. The actual deprojection starts from 87 kpc. The assumption that the 130-kpc bin

is mostly background and is not contributing to the cooling flow emission is justified, because the cooling radius (inside which the cooling time is less than 2×10^{10} yr) is about 90 kpc, and the surface brightness at 130 kpc is three orders of magnitude less than at the outer deprojection bin, 87 kpc. In order to increase the signal-to-noise ratio of the data, the profile was rebinned into 2-arcmin bins.

The potential is constrained by the optical velocity dispersion ~ 310 km s^{-1} (Roberts et al. 1991), but the shape is a variable input parameter. We have investigated the difference between assuming that the gravitating matter follows a true isothermal potential or a de Vaucouleurs distribution. The cluster velocity dispersion is taken as 400 km s^{-1} (Edge & Stewart 1991). The effects of varying this and of omitting the cluster as a source of gravitating mass are also investigated.

We use the Galactic column density of 1.3×10^{20} cm^{-2} for the deprojection, and no extra absorption at the source, consistent with the RS spectral results.

3.3 Deprojection results

In general, the deprojection results agree well with the previous deprojection done using the *Einstein* HRI observation (White 1992). The order-of-magnitude increase in counts over the latter data, at a similar spatial binning, means that the temperature, cooling time and mass deposition rate are enormously better constrained by the *ROSAT* data. The surface brightness is a much stronger function of density than temperature, so the density is always much better constrained. Similarly, the pressure is well constrained, as it is mostly determined by the weight of the shells of gas above, and thus the density. We agree with the HRI density and pressure profiles. The temperature and pressure profiles are given in Figs 8 and 9, respectively.

The shape of the gravitating mass distribution was adjusted to bring the temperature profile into agreement with the spectrally determined temperature profile using RS models, as used in the deprojection software. This sets strong constraints on the gravitating matter.

Both galaxy potential shape (true isothermal and de Vaucouleurs distributions) and shape parameters (r_e, r_c) were varied, and both galaxy potentials were tested with and without the presence of a cluster potential. The effect of this was to produce several parametrizations of the same gravitating mass profile. The cluster potential is not constrained at all, because all our high signal-to-noise observations are well within the cluster core radius. The use of a cluster potential merely changes the parametrization.

The gravitational and gas masses derived by the deprojection analysis are presented in Fig. 10, and the different parametrizations of the potential are listed in Table 2. The de Vaucouleurs core radii are larger than normally quoted for cD galaxies, and these potentials were harder to fit than the isothermal ones. Isothermal potentials either with or without being in a cluster potential were the most stable fit with regard to changes in core radius. R_e and R_c can vary by up to 20 per cent before the temperature profiles become noticeably non-isothermal.

In the central 8-kpc bin of NGC 1399 the gas mass is ~ 0.1 per cent of the gravitational mass, rising to 1 per cent within 80 kpc. This illustrates how the gravitating mass is

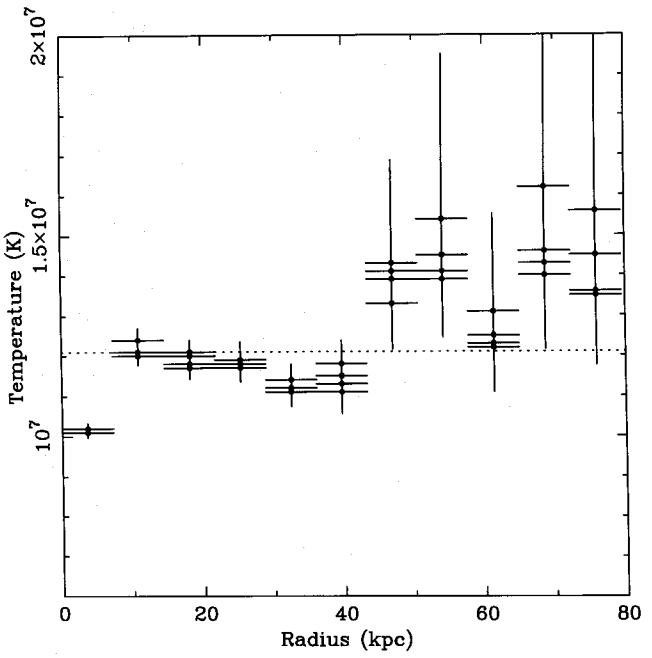

Figure 8. The temperature profile of the X-ray-emitting gas around NGC 1399 derived by deprojection. Points are medians, with error bars at the 10th and 90th percentiles. Note that, because the deprojection code uses RS plasma models, the deprojection outer pressure was normalized so that this temperature profile was in agreement with the spectrally derived temperatures using RS models (Fig. 3). The four sets of points are derived from the four potential models used.

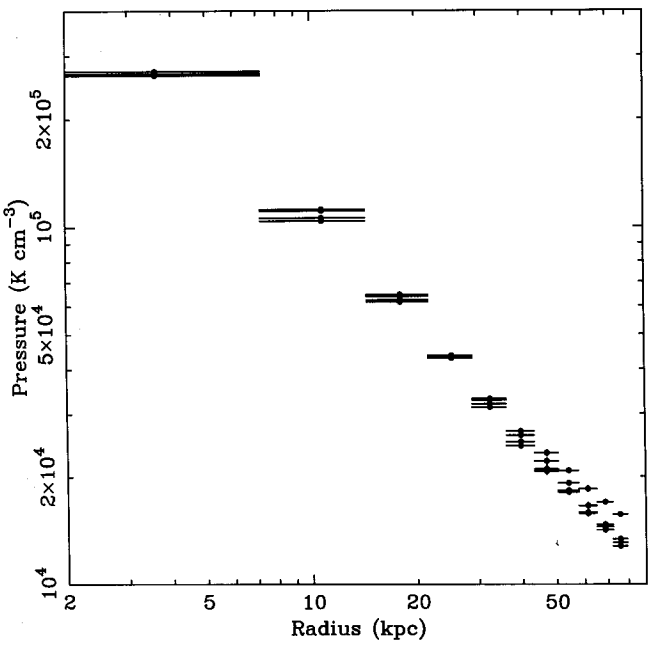

Figure 9. The pressure in the X-ray-emitting gas around NGC 1399 derived by deprojection. Note that these are likely to be lower limits within 40 kpc due to the extra cold gas column density observed. The four sets of points are derived from the four potential models used.

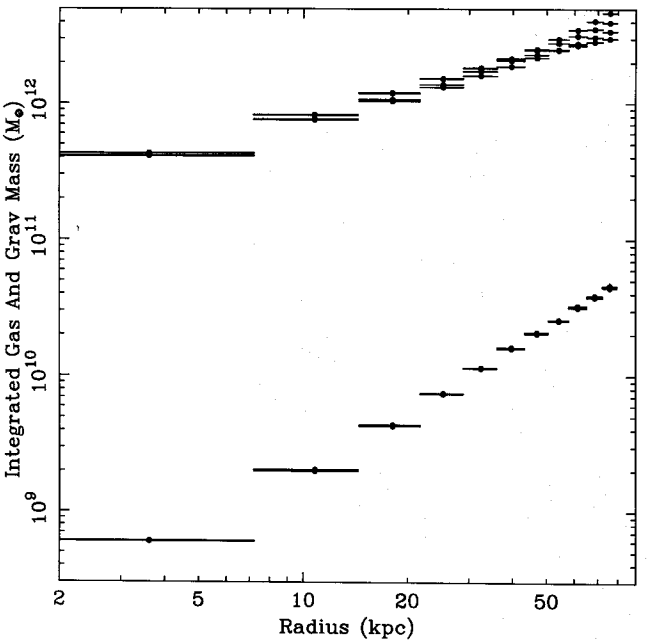

Figure 10. Integrated gas mass (lower points) and gravitational mass (upper points) in NGC 1399 as a function of radius, from the deprojection of NGC 1399. Note that the gas mass is likely to be a lower limit within 40 kpc due to the extra cold gas column density observed using the spectral models. The four sets of points are derived from the four potential models used.

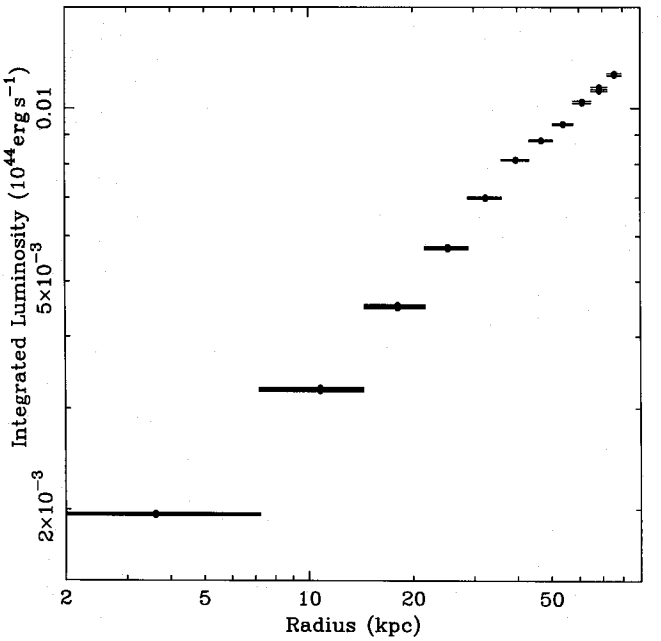

Figure 11. Integrated bolometric X-ray luminosity of NGC 1399. The four sets of points are derived from the four potential models used. Because the deprojection parameters are derived from the surface brightness profile, this luminosity profile is highly model-independent.

Table 2. Gravitating mass distribution parameters for the best-fitting deprojection potential.

Galaxy model	Cluster model	Gal. R_c kpc	Gal. R_e kpc	Cluster R_c kpc	P_0 10^4 K cm^{-3}
Iso T	Iso T	2		200	1.1
Iso T	-	2			1.4
D V	Iso T		40	200	1.1
D V	-		50		1.2

Iso T is a true isothermal potential. D V is a de Vaucouleurs potential. P_0 is the outer pressure assumed, at 87 kpc. The galaxy velocity dispersion used was 310 km s^{-1}, and the cluster velocity dispersion was 400 km s^{-1}.

primarily on galaxy scales, while the gas (1.1 keV), being hotter than the virial temperature of the galaxy (0.85 keV), is more diffuse and spreads out on cluster scales. The mass in gas within 40 kpc, $M_{\rm gas}(<40\ {\rm kpc}) \sim 1.5\times10^{10}\ {\rm M}_\odot$, which is ~28 per cent of the stellar mass, and ~0.75 per cent of the gravitating mass.

The bolometric X-ray luminosity calculated from the deprojection (8×10^{41} erg s^{-1} within 40 kpc which gives 4.6×10^{41} erg s^{-1} in the range 0.5–4.5 keV) agrees to within 5 per cent with published X-ray luminosities (Roberts et al. 1991) from the *Einstein* IPC (4.4×10^{41} erg s^{-1} in the range 0.5–4.5 keV), and with the luminosity derived from the PSPC image directly. The radial profile of luminosity is shown in Fig. 11.

In the central 8 kpc of NGC 1399, the density is 0.014 cm^{-3}, falling to $(4.6\pm0.1)\times10^{-4}$ cm^{-3} at a radius of 80 kpc (Fig. 12). The effect of mass loss by stars is shown in the plot as a dotted line indicating the amount of gas at each radius that would be deposited by the stars, assuming that the average stellar mass loss for a galaxy the size of NGC 1399 is $\dot{M}_{\rm stellar}(<40\ {\rm kpc}) \sim 0.8\ {\rm M}_\odot\ {\rm yr}^{-1}$ (Faber & Gallagher 1976) and operates for 10^{10} yr. This mass injection rate is assumed to be proportional to the current stellar density derived from the optical surface brightness. Killeen & Bicknell (1988a) find that the stellar B-band surface brightness follows a power law, index −1.7, so we assume a stellar density $\sim r^{-2.7}$, and a total mass loss rate of 0.8 M$_\odot$ yr^{-1}.

Fig. 13 shows the cooling time, the time taken for the gas to radiate away most of its thermal energy. $t_{\rm c,central} \sim 3.6\times10^8$ yr, similar to that found in the centre of much larger cluster cooling flows such as Abell 478 (Allen et al. 1993). The cooling radius (within which $t_{\rm c}<2\times10^{10}$ yr) is $r_{\rm c}\sim90$ kpc ~ 12 arcmin, only just larger than the galaxy itself, and an order of magnitude smaller than the detected extended X-ray emission. The profile has small error bars, because $t_{\rm c}$ is derived primarily from the count emissivity for each shell, and depends otherwise only on the integral of the pressure, which is well constrained.

The mass deposition rate (Fig. 14) for the cooling flow is $\dot{M}=1.9\pm0.1\ {\rm M}_\odot\ {\rm yr}^{-1}$ within 40 kpc, and another 0.7 ± 0.7 M$_\odot$ yr^{-1} from 40 kpc out to the cooling radius. The main cooling flow is located within 40 kpc, i.e., inside the galaxy itself. The distinction between the cluster cooling flow and the galaxy cooling flow appears to be more than semantic –at

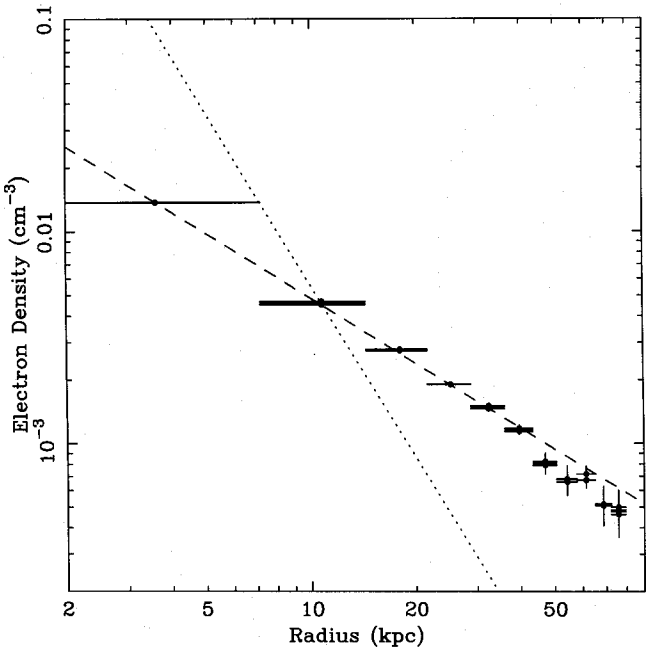

Figure 12. The electron density in the X-ray-emitting gas around NGC 1399 derived by deprojection. The dotted line shows the integrated mass loss over 10^{10} yr by stellar mass loss at a canonical rate. The dashed line is a power-law fit to the density, with a gradient of -1.02. Note that these are likely to be lower limits within 40 kpc due to the extra cold gas column density observed. The four sets of points are derived from the four potential models used. Because the emissivity is a strong function of density, and the deprojection parameters are derived from the surface brightness profile, this density profile is highly model-independent.

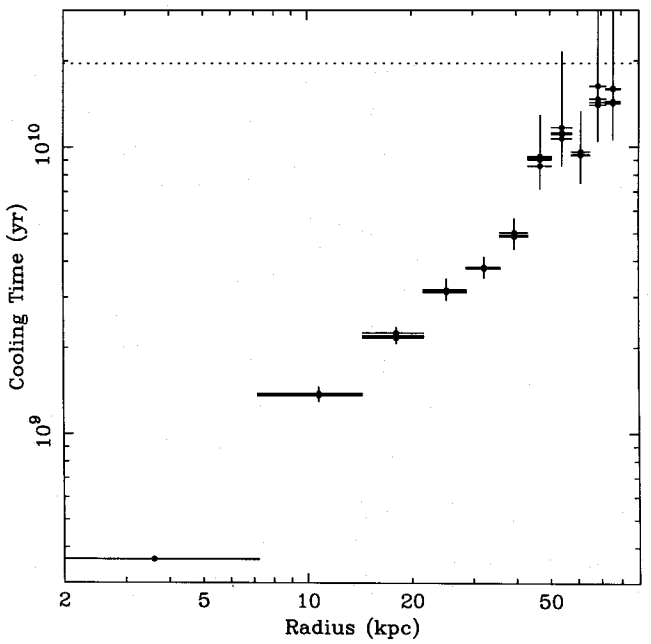

Figure 13. The cooling time in the X-ray-emitting gas around NGC 1399 derived by deprojection. Points are medians, with error bars at the 10th and 90th percentiles. Note that these are likely to be upper limits within 40 kpc due to the extra cold gas column density observed. The four sets of points are derived from the four potential models used.

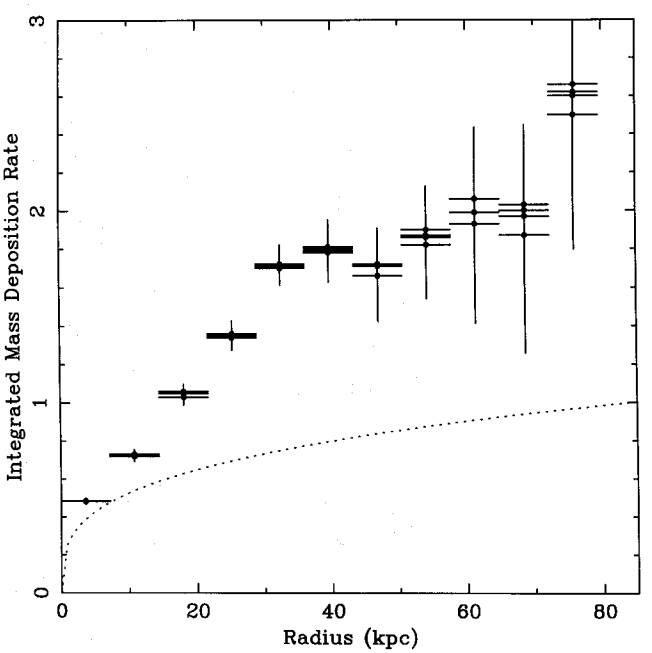

Figure 14. The integrated mass deposition rate of the cooling flow in NGC 1399 derived by deprojection. Points are medians, with error bars at the 10th and 90th percentiles. The four sets of points are derived from the four potential models used. Also plotted (the dotted line) is the expected stellar mass-loss rate within each radius, assuming a total mass-loss rate for the galaxy of 0.8 $M_\odot$ yr^{-1} within 40 kpc and a stellar density $\sim r^{-2.7}$ (see text). Units are $M_\odot$ yr^{-1}.

40 kpc the mass deposition rate, cooling time, electron density, and cold gas column density all change distinctly, and indicate that within the galaxy more cooling is taking place than would be extrapolated from the cluster cooling flow outside 40 kpc. The uncertainties in the mass deposition rate at radii >40 kpc are due to the low surface brightness, and not to uncertainties in the potential, as all the potentials tried had similar deposition rates with similar errors in the outer regions. The plot also shows the stellar mass injection rate, derived from the optical surface brightness as above – if the stellar density $\rho_{\rm stellar} \sim r^{-2.7}$, then the integrated stellar mass-loss rate, $\dot{M}_{\rm stellar}(<r) \sim \int_0^r \rho_{\rm stellar} r^2 {\rm d}r \sim r^{0.3}$, normalized to be 0.8 $M_\odot$ yr^{-1} within 40 kpc. The cooling flow mass deposition rate is always greater than the stellar mass-loss rate, even in the innermost bins.

4 DISCUSSION

The integrated mass of absorbing gas, derived from the absorption profile (Fig. 6), is 1.64×10^{10} $M_\odot$ out to 40 kpc in the galaxy, assuming a solar abundance in the absorbing gas. If the abundance is higher, then the mass will be correspondingly lower. Note that because of the mass of cold gas in the inner 10 kpc, which is not included in the model used in the deprojection, the deprojection results within 10 kpc need to be adjusted. The density, pressure and mass deposition rates are then higher than shown, and the cooling time lower. The discussion below treats these values as upper or lower limits as necessary. Because of the added complication of the cold gas weight, more detailed and complex

deprojections have not been attempted, and will be unconstrained until the mass fraction of each gas phase as a function of radius is well defined.

The mass of hot gas is 1.6×10^{10} $M_\odot$ out to 40 kpc (Fig. 10). The absorption profile out to 40 kpc was fitted with a power law (shown in Fig. 6), and gives $N_H\sim4\times10^{21}(r/\mathrm{kpc})^{-0.95}$ cm^{-2}, implying that the density of absorbing gas $n_{H_{cold}}\sim1.3(r/\mathrm{kpc})^{-1.95}$ particle cm^{-3}. Integrating this, we obtain a mass $M_{cold}(<r)\sim3.4\times10^8(r/\mathrm{kpc})^{1.05}$. This is intriguingly similar to the distributed mass deposition profile found in many clusters, where $\dot{M}(<r)\sim r^\alpha$ and $\alpha\sim1$–2 (Thomas, Fabian & Nulsen 1987; Fabian, Nulsen & Canizares 1991; White et al. 1991). Because of stellar mass loss, one would expect the cold gas density gradient to be flatter than the cluster mass deposition profile, assuming that a similar cooling flow mechanism is operating. The similar profiles may indicate that the efficiency of gas removal by star formation is constant with changing cold gas density over this density range – if it was a strong function of density, the profile would be much flatter.

A comparison of the cooling flow and stellar mass injection rates in the integrated mass deposition profile (Fig. 14) and the electron density profile (Fig. 12) shows clearly the mass flows and sinks in the galaxy. In the centre $\dot{M}_{stellar}<\dot{M}_{cooling\,flow}$, but even the stellar mass loss alone is enough to fill the central 10 kpc with the amount of gas, both hot and cold, that is seen in the density profile: $M_{hot}(<10$ kpc$)\sim2\times10^9$ $M_\odot$ (Fig. 10), $M_{cold}(<10$ kpc$)\sim4\times10^9$ $M_\odot$, $\dot{M}_{stellar}(<10$ kpc$)\sim0.53$ $M_\odot$ yr^{-1}. For arguments using the total amount of mass and mass flows within some radius to be valid, the volume that is considered must be fairly homogeneous, as large gradients will introduce weighting factors ~1. For example, the volume must not be divisible into one part where cold gas predominates and one where hot gas is dominant. The time it takes for gas at ~100 km s^{-1} to move 10 kpc is $\sim10^8$ yr, so the central 10 kpc should be a sufficiently intermixed gas mass, despite the potential gradient, for these arguments to hold.

In addition to this gas injection, the cooling flow mass injection detected in the centre $\dot{M}_{cooling\,flow}(<10$ kpc$)\sim0.5$ $M_\odot$ yr^{-1}, so star formation must have removed several $\times10^9$ $M_\odot$ from the ISM of the central 10 kpc over 10^{10} yr, even allowing for a higher abundance, and so a lower mass of the cold gas. The cooling flow mass injection is, in fact, likely to be higher than derived here, because the extra cold gas is not included in the cooling flow calculation, so it will increase the density of the gas, and the mass deposition rate. The current mass in stars within 10 kpc is 3.5×10^{10} $M_\odot$, using the same stellar density distribution as above, a stellar mass-to-light ratio of $M/L=1$, similar to the Milky Way bulge stars (Kent 1992), and $\log L(B_0)=10.72$ $L_\odot$ (Roberts et al. 1991). If the mass-to-light ratio of the stars is higher, then, of course, there may be a higher mass of stars in the galaxy, but even using $M/L=1$ the current stellar mass is much larger than the mass of stars that may have been produced by the deposited gas.

The possibility that there has been an outflowing wind, to redistribute the gas from the centre further out and flatten the accumulated stellar mass-loss profile to the same gradient as the density profile, seems unlikely here because of the surface brightness profile (Fig. 7) – an outflowing wind is only stable when supersonic and thus should have a density $\sim r^{-2}$, giving a surface brightness profile $\sim r^{-3}$ (the emissivity $\sim\rho^2T^{0.5}$, so temperature gradients play little role in the brightness profile).

In summary, the total amount of gas injected into the central 10 kpc of NGC 1399 over 10^{10} yr (the sum of stellar mass loss and the cooling flow mass deposition) is more than is detected in any gas phase, and so there must have been gas removal, probably by star formation. Away from the core of the galaxy, outside 10 kpc, $\dot{M}_{stellar}$ is too small to explain the high density (Fig. 12), and this shows that there must have been an inflow of gas from the cluster core. The high cooling flow mass deposition rate (Fig. 14) at radii greater than 20 kpc is a result of the higher density, because the whole cluster is close to isothermal.

From Fig. 12, the density of hot gas $\sim r^{-1.02}$, thus giving a column density $N_{hot}\sim r^{-0.02}$. This is plotted in Fig. 6, normalized so that the column density is the Galactic H I value at 35 kpc (the intercept of the cold gas column density with Galactic column) so that the Galactic column density line is effectively a zero-line, giving $N_{hot}\sim7.7\times10^{21}(r^{-0.02}-35^{-0.02})$ cm^{-2} for r in kpc. This allows easy comparison of the hot and cold gas column densities within 35 kpc; for example, the hot column density at $r=2$ kpc is 6.2×10^{20} cm^{-2}, whereas the cold gas density is about 2×10^{21} cm^{-2}, integrating inwards from 35 kpc. However, the hot gas column density is derived from deprojection analysis, which does not include the extra weight of the cold gas in its calculation, so the pressure and density plots must be treated as lower limits within 40 kpc. Thus the cooling time may well be lower, and the mass deposition rate higher than shown. Even allowing for this, it is clear that the densities of cold and hot gas at each radius are approximately equal, within 40 kpc of the centre of NGC 1399. This must be near the limits of what the hot gas can support without being convectively unstable, or cooling catastrophically quickly in the centre, because of the high density.

The spectral shape of the excess very soft emission needed in the models is not constrained by the data, and thus its source is speculative, but it seems likely to be connected with the stellar density. One possibility is that it could be the integrated emission of dwarf M and K stars. The flux in the soft model component has a high upper limit, because a small increase in the absorption is enough to compensate for a large increase in soft flux. A lower limit (90 per cent probability) on the soft flux is $\sim5\times10^{40}$ erg s^{-1} (0.2–2 keV) within 40 kpc, which corresponds to a flux on our Galaxy of order 8×10^{40} erg s^{-1} (with the Galactic absorption effect subtracted off). This requires over 10^{13} stars, assuming an average X-ray luminosity of 3×10^{27} erg s^{-1} (Barbera et al. 1993), obviously more than the number of stars present. Thus we do not believe that the soft component is dominated by stellar X-ray emission. The soft component could be stellar mass-loss ejecta. The highly multiphase stellar wind, thrown into the ISM at vastly different velocities by different stars, will probably produce a very multiphase mixture with the ISM, and not all will be shock-heated up to the maximum hot thermal component temperature. A part could easily be heated up to a few million K, cool quickly and so show a strong cool thermal component with a very small volume filling factor. The mass cooling rate from 2×10^6 K required to emit the soft flux at 8×10^{40} erg s^{-1} is ~1.6 $M_\odot$ yr^{-1}, assuming the gas gives off $5kT/2$ per particle as it cools in pressure equilibrium. This is less than the sum of the stellar

mass-loss rate ($0.8\ M_\odot\ yr^{-1}$) and the cooling flow mass deposition rate within 40 kpc ($2\ M_\odot\ yr^{-1}$). An explanation of the soft flux may be that it is a combination of stellar X-ray emission, emission by the coolest gas from the cooling flow, and cooling by a part of stellar mass loss, shock-heated up to a few million K.

It is possible that the model is incorrect, and the goodness of fit of the two-temperature models is merely an artefact of the spectral resolution of the detector. However, it should be emphasized that the main thermal component temperature determinations are little affected by these model changes – the temperature is extremely well determined by the spectra above 1 keV, and the model changes are negligible at high energies. The high column density found in the centre of the galaxy is also a robust result, as it is dependent on fitting the spectra above 1 keV.

The spectra from the inner 40 and 10 kpc fit simple cooling flow spectra, with an acceptable reduced chi-squared of $\chi^2/\nu = 1.1$. The mass deposition rate in the inner 40 kpc is $\dot{M}_{\rm spectral} \sim 1.6\ M_\odot\ yr^{-1}$, and up to $1\ M_\odot\ yr^{-1}$ in the inner 10 kpc. However, because of the lack of spectral resolution, the solutions are degenerate; so while both cooling flows and simple two-component models fit acceptably, the errors on them are indeterminate. This set of emission and absorption processes is much too complex and degenerate for these spectra to find the relative amounts of the soft flux due to the cooling flow, stellar mass loss, and stars themselves.

One possible modification to the deprojection method is to introduce supernova energy injection and stellar mass injection (Thomas et al. 1986). This reduces the mass deposition rate by up to 30 per cent for a cooling flow of this size, but relies on the assumption of the supernova rate (up to that of Tammann 1974). Smaller cooling flows, where the mass deposition rate is of the order of the stellar mass injection rate, change greatly in dynamics and mass flow, but because the mass inflow rate is twice the stellar mass injection rate for NGC 1399, all solutions still have inflow, mass deposition, and short central cooling times. Because of uncertainty in both current and previous star formation rates the supernova rate in NGC 1399 is very poorly known, but the amount of cooling gas could be reduced to a total of about $2\ M_\odot\ yr^{-1}$ if the supernova rate is high. Because the uncertainties in the input parameters are high, and the introduction of mass and energy injection into the deprojection does not change the results by more than 30 per cent, we do not include the effects of mass injection directly in the deprojection.

The *HUT* observations (Ferguson et al. 1991) allow only low-mass star formation. Efficient low-mass star formation is a possibility mooted for many cooling flows, to account for the level of cool gas observed (Nulsen, Stewart & Fabian 1984), and it can explain the discrepancy between the maximum amount of cool gas that could be present and the observed amount in NGC 1399. However, both the BBXRT and these models do detect excess absorption in NGC 1399, and so the star formation cannot be so efficient as to remove all the absorbing clouds. The maximum rate must therefore be below about $2\ M_\odot\ yr^{-1}$ in the galaxy over the lifetime of the galaxy.

It is possible to hide an order of magnitude more absorbing gas from detection by the PSPC if it only partially covers the emitting plasma, because of the low number of spectral channels in the PSPC data. The soft flux must rise to compensate for the extra absorption, and thus it seems unlikely that the column density could be more than 10^{22} cm^{-2} even if partially covering. A detector with better sensitivity in the 0.1–0.8 keV band should be able to distinguish if this is the case. Because NGC 1399 is very bright in the carbon band, and spillover from this into the 0.3–0.5 keV band reduces the sensitivity of the *ROSAT* PSPC data to partial covering, the BBXRT should be more sensitive to absorbing gas partially covering the emitting 1-keV plasma.

Given the problems known to exist with the *ROSAT* PSPC response matrix around 0.2–0.4 keV, results dependent on fits using Pulse Height Analyser (PHA) channels below 0.5 keV should be viewed with caution. This is particularly so in observations of cool sources, with high signal-to-noise ratios. We note, however, that to allow acceptable fits without a soft component in the inner 40 kpc of NGC 1399 would require systematic errors at the 10 per cent level, which is larger than those currently thought possible, and the large absorbing column densities detected are not dependent on the data below 1 keV.

If the gas around NGC 1399 is not in hydrostatic equilibrium, then the deprojection analysis applied would be invalid, but the excellent agreement between deprojected temperature profile and spectrally determined temperature profile using a plausible gravitational potential implies that, in fact, hydrostatic equilibrium is a good approximation. The surface brightness profile is not one that can easily be reconciled with models of the ISM as outflowing winds or a central hot bubble.

The presence of magnetic fields entangled in the plasma may alter the temperature and density profiles of the gas, but Soker & Sarazin (1990) show that, if the magnetic field is never stronger than equipartition with the thermal energy of the plasma, the attributes of the cooling flow are not greatly altered.

Thus the X-ray absorption measured with the PSPC is consistent with the cooling flow mass loss, stellar mass injection rate, observed absorption with the BBXRT, and *HUT* ultraviolet star formation constraints. More absorbing gas can exist undetected in NGC 1399 if distributed patchily, in clumps partially covering the emitting hot plasma from our line of sight. Some gas must have been removed by star formation over the lifetime of the galaxy, and, if the same mechanism is operating now, the IMF of the stars formed must be truncated, with many more low-mass stars. The gaseous environment in ellipticals appears to be vastly more complex than that of clusters, and simple scaling laws and models derived from studies of the intracluster medium are not directly applicable. The amount, temperature and phase of stellar mass loss, the effect of any cooling flow from the surrounding cluster and internally, and star formation all complicate the ISM of elliptical galaxies, and make a unified model a highly desirable, if difficult, objective.

5 SUMMARY

Using a *ROSAT* PSPC observation of the central cluster galaxy NGC 1399, we have derived spectrally determined temperature profiles to high accuracy within 330 kpc, and set limits on the absorption present. We have deprojected the surface brightness profiles and derived a consistent set of

physical parameters to describe the X-ray-emitting gas within 80 kpc.

We have shown that the gas in the cluster is basically isothermal, at a temperature of 1.1 ± 0.1 keV for RS models, and 0.9 ± 0.1 keV for MEKA models. The temperature in the centre falls to 0.85 keV (RS) or 0.6 keV (MEKA). The gas in the central 40 kpc has a cooling time below 4×10^9 yr, and a mass deposition rate of almost $2\,M_\odot\ yr^{-1}$. This area needs a two-temperature spectral model with a soft component to fit adequately, and the MEKA models need high column densities of $\sim 2 \times 10^{21}$ cm^{-2} to match the spectral shape at around 1 keV from the inner 1 arcmin. Cooling flow spectral models fit the central few kpc adequately, but the spectra do not have sufficient resolution to distinguish between the soft thermal and cooling flow components.

The spectra show no radial abundance gradient and are always consistent with solar abundance. The radio nucleus is not detected, and its X-ray flux (0.2–2 keV) is less than 2.4×10^{-13} erg cm^{-2} s^{-1} at 90 per cent confidence (using the RS models), corresponding to a band luminosity of 2×10^{40} erg s^{-1} at source.

We have shown profiles for many physical parameters, including the excess cold column density, hot X-ray-emitting gas density, pressure, gravitating mass and temperature. Within 10 kpc, the mean density of cold absorbing gas appears to be similar to that of the hot gas. This combination of analyses shows that the gaseous evolution of NGC 1399 has been characterized by steady gas inflow and cooling, with a cooling flow operating largely within the galaxy, and the build-up of cool gas within the galaxy.

ACKNOWLEDGMENTS

We thank Steven Allen, David White, David Helfand, Paul Nulsen, John Pye and Roderick Johnstone for useful criticism and discussions. ACF thanks the Royal Society for support.

REFERENCES

Allen S. W., Fabian A. C., 1994, MNRAS, 269, 409
Allen S. W., Fabian A. C., Johnstone R. M., White D. A., Daines S. J., Edge A. C., Stewart G. C., 1993, MNRAS, 262, 901
Anders E., Grevesse N., 1989, Geochim. Cosmochim. Acta, 53, 197
Arnaud M., Raymond J., 1992, ApJ, 398, 394
Barbera M., Micela G., Sciortino S., Harnden F. R. Jr., Rosner R., 1993, ApJ, 414, 846
Bridges T. J., Hanes D. A., Harris W. E., 1991, AJ, 101, 469
Edge A. C., Stewart G. C., 1991, MNRAS, 252, 428
Faber S. M., Gallagher J. S., 1976, ApJ, 204, 365
Fabian A. C., Hu E. M., Cowie L. L., Grindlay J., 1981, ApJ, 248, 47
Fabian A. C., Nulsen P. E. J., Canizares C. R., 1991, A&AR, 2, 191
Ferguson H. C. et al., 1991, ApJ, 382, L69
Hasinger G., 1992, in Barcons X., Fabian A. C., eds, The X-ray background. Cambridge Univ. Press, Cambridge, p. 229
Ikebe Y. et al., 1992, ApJ, 384, L5
Jenkins C. R., 1983, MNRAS, 205, 1321
Jura M., 1986, ApJ, 306, 483
Kaastra J. S., Mewe R., 1993a, Legacy - HEASARC, 1993 May, No. 3, p. 16
Kaastra J. S., Mewe R., 1993b, A&AS, 97, 443
Kent S. M., 1992, ApJ, 387, 181
Killeen N. E. B., Bicknell G. V., 1988a, ApJ, 325, 165
Killeen N. E. B., Bicknell G. V., 1988b, ApJ, 325, 180
Kim D.-W., Fabbiano G., Trinchieri G., 1992, ApJS, 80, 645
Mewe R., Groenenschild E. H. B. M., van den Oord G. H. J., 1985, A&AS, 62, 197
Morrison R., McCammon D., 1983, ApJ, 270, 119
Nulsen P. E. J., Stewart G. C., Fabian A. C., 1984, MNRAS, 208, 185
Raymond J. C., Smith B. W., 1977, ApJS, 35, 419 (RS)
Roberts M. S., Hogg D. E., Bregman J. N., Forman W. R., Jones C., 1991, ApJS, 75, 751
Sadler E. M., Gerhard O. E., 1985, MNRAS, 214, 177
Sadler E. M., Jenkins C. R., Kotanyi C. G., 1989, MNRAS, 240, 591
Serlemitsos P. J. et al., 1991, in Tanaka Y., Koyama, K., eds, Frontiers of X-ray Astronomy, Proc. Yamada Conference, 1991. Universal Academy Press, Nagoya, Japan, p. 221
Serlemitsos P. J., Loewenstein M., Mushotzky R. F., Marshall F. E., Petre R., 1993, ApJ, 413, 518
Soker N., Sarazin C. L., 1990, ApJ, 348, 73
Stark A. A., Gammie C. F., Wilson R. W., Bally J., Linke R. A., Heiles C., Hurwitz M., 1992, ApJS, 79, 77
Tammann G. A., 1974, in Cosmovici C. B., D'Anna E., Borghesi A., eds, Supernovae and Supernova Remnants. Reidel, Dordrecht, p. 155
Thomas P. A., Fabian A. C., Arnaud K. A., Forman W. R., Jones C., 1986, MNRAS, 222, 655
Thomas P. A., Fabian A. C., Nulsen P. E. J., 1987, MNRAS, 228, 973
Turner T. J., George I. M., 1992, NASA OGIP Calibration Memo CAL/ROS/92-001
White D. A., 1992, PhD thesis, Univ. Cambridge
White D. A., Fabian A. C., Johnstone R. M., Mushotzky R. F., Arnaud K. A., 1991, MNRAS, 252, 72
White D. A., Fabian A. C., Allen S. W., Edge A. C., Crawford C. S., Johnstone R. M., Stewart G. C., Voges W., 1994, MNRAS, 269, 589